Temperature Trend of the Last 40 Yr in the Upper Pacific Ocean

BOYIN HUANG AND ZHENGYU LIU

Department of Atmospheric and Oceanic Sciences, University of Wisconsin—Madison, Madison, Wisconsin

(Manuscript received 11 February 2000, in final form 2 February 2001)

ABSTRACT

The linear temperature trend of the last 40 yr (1955–94) in the upper Pacific Ocean above 400 m is studied using an objectively analyzed dataset and simulations of an ocean general circulation model. Both the data and simulations suggest a warming trend in the western tropical Pacific (10°S–10°N) near the surface and in the eastern tropical Pacific above 400 m but a cooling trend in the thermocline of the western tropical Pacific. In the midlatitude North Pacific (30°–50°N), the temperature trend is positive east of 150°W but negative to the west.

Simulated heat budget indicates that the temperature trend in the tropical Pacific may result from oceanic advection. In the central and western Pacific, the surface warming is associated with the reduction of cold advection from the off-equatorial divergent flow and the South Equatorial Current, while the cooling in the thermocline is related to the reduction of equatorward warm advection. In the eastern Pacific, the warming is associated with the reduction of upwelling. The reduction of these ocean currents, in turn, may result largely from the weakening of the trade winds.

In the midlatitude North Pacific, the ocean temperature trends similarly may result from the oceanic advection associated with the reduction of the westerlies. The effect of net surface heat flux into the ocean is a damping factor to the sea surface temperature. These studies highlight the importance of oceanic advection in producing long-term temperature trends.

1. Introduction

Based on observations of sea surface temperature (SST) of the Comprehensive Ocean–Atmosphere Data Set (COADS; da Silva et al. 1994) during the last 50 yr, it is found that there is a warming trend in the tropical Pacific, a cooling trend in the North Pacific west of 140°W between 20° and 50°N, and a cooling trend east of Australia in the South Pacific (Fig. 1a; also see Latif et al. 1997; Knutson and Manabe 1998; Curtis and Hastenrath 1999). The mechanisms responsible for the long-term temperature trends, however, are not well understood. The SST trend does not seem to result directly from net surface heat flux in most regions, especially in the tropical Pacific where the net surface heat flux derived from the COADS exhibits a negative trend (Fig. 1b). The inconsistency between the trends of the SST and net surface heat flux suggests that the SST trend may not be directly associated with the net surface heat flux, although there is a large uncertainty in the calculated surface heat fluxes. This raises the question: What mechanisms lead to the warming and cooling of the ocean? Further, there have been few studies on the subsurface temperature trend. Questions of interest include: What is the trend of the oceanic temperature below the surface during the past 50 yr, and what are the mechanisms for this trend?

In this work, the linear trend of ocean temperature is derived in the tropical Pacific and midlatitude North Pacific, using both an objectively analyzed dataset and an ocean general circulation model (OGCM). The model simulation also enables us to analyze the heat budget. It is found that the ocean temperature trends are associated largely with oceanic advection. The paper is organized as follows: the data and OGCM are briefly described in section 2. The temperature trends from the data and simulations in the Pacific Ocean above 400 m are presented in section 3. The physical mechanisms are studied by analyzing the heat budget in the tropical Pacific in section 4, and in the midlatitude North Pacific in section 5. Sections 6 and 7 are the discussion and conclusions.

2. Data and OGCM

The monthly mean temperature data in the upper 400 m between 1955 and 1994 (White 1995) are used to derive the linear trend of ocean temperature. The data are produced objectively from the National Oceanographic Data Center (NODC) Global Ocean Tempera-

Corresponding author address: Dr. Boyin Huang, Department of Earth, Atmospheric, and Planetary Sciences, Massachusetts Institute of Technology, Room 54-1721, 77 Massachusetts Ave., Cambridge, MA 02139.
E-mail: bhuang@wind.mit.edu

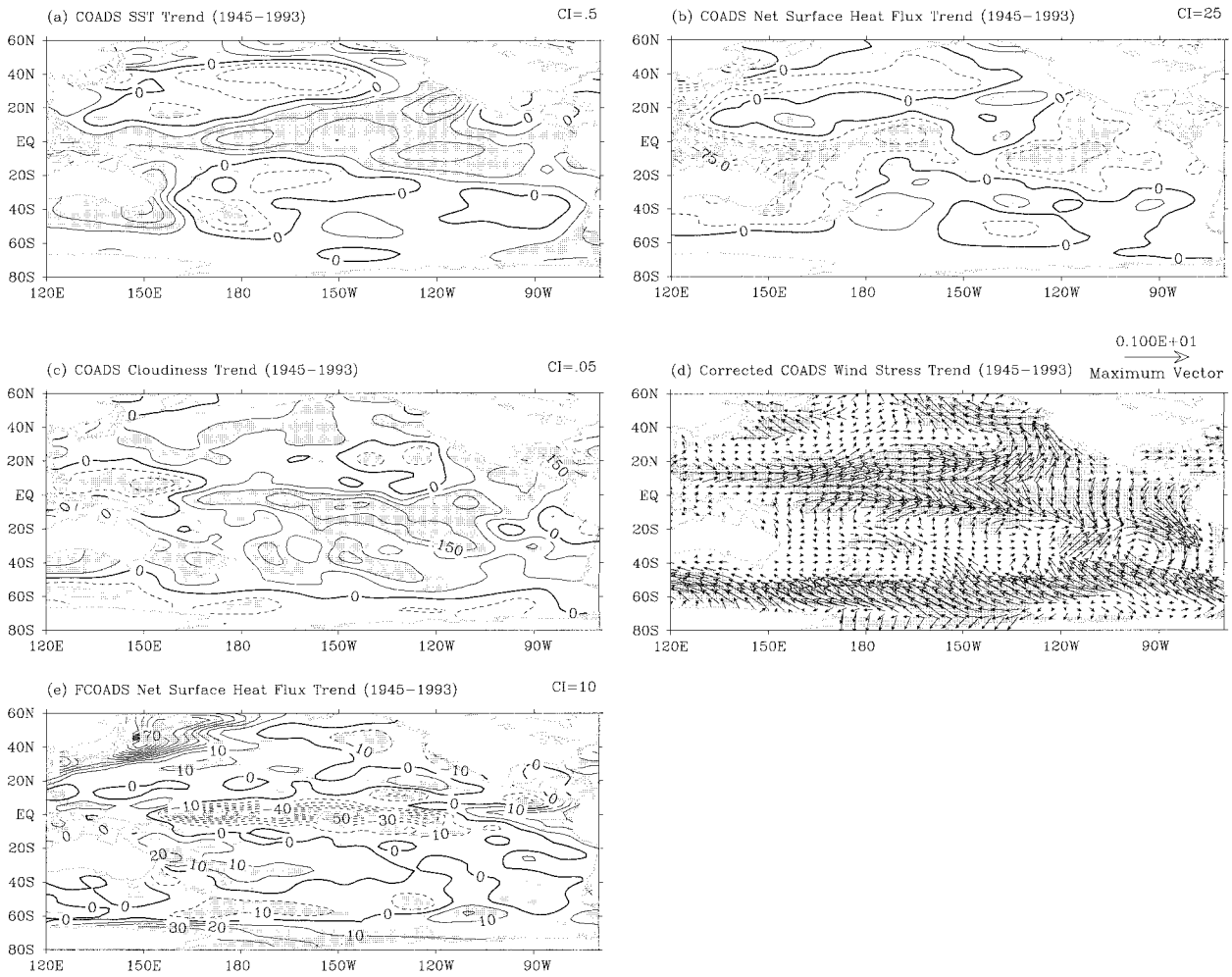

FIG. 1. Linear trends (1945–93) of (a) COADS SST, (b) COADS net surface heat flux into the ocean, (c) COADS cloudiness, (d) corrected wind stress, and (e) net surface heat flux in the FCOADS run. The contour interval (CI) for (a)–(c) is 0.5 K century^{-1}, 25 W m^{-2} century^{-1}, and 0.05 century^{-1}, the unit in (d) is dynes per square centimeter per century, and for (e) the CI is 10 W m^{-2} century^{-1}. Solid (dashed) contours denote positive (negative) values. Shaded region indicates that the confidence level is higher than 95%.

ture–Salinity CD-ROM dataset between 1955 and 1988 and Global Temperature–Salinity Pilot Product (GTSPP) dataset between 1989 and 1993 (Chepurin and Carton 1999), with a resolution of 4° lat × 5° long. The NODC and GTSPP datasets include available historic in situ observations of mechanical bathythermographs, expendable bathythermographs, conductivity-temperature-depth probes, and bottle casts (Robinson et al. 1979; Levitus and Gelfeld 1992; Levitus and Boyer 1994). There are relatively few observations below 150 m before the late 1960s (Giese and Carton 1999). Since the data are sparsely sampled south of 20°S, our major focus will be on the tropical and North Pacific.

The Geophysical Fluid Dynamics Laboratory Modular Ocean Model (MOM2 beta; Pacanowski 1996) is used in our study. The model domain extends globally from 80°S to 60°N, with a horizontal resolution of 2° × 2° and 30 vertical levels. The level thickness is 25 m between the depth of 0 and 400 m and linearly increases to 550 m at the bottom layer (5500 m). The horizontal and vertical viscosities are 10^4 and 10^{-4} m^2 s^{-1}, respectively, while the horizontal and vertical diffusivities are 10^3 and 10^{-5} m^2 s^{-1}, respectively.

The model ocean is driven by the wind stress, net incoming solar radiation, net outgoing longwave radiation, and sensible and latent heat fluxes between the ocean and atmosphere. The wind stress is calculated using COADS wind velocities. The net incoming solar radiation is a function of surface albedo and total cloudiness in COADS (da Silva et al. 1994). The net longwave radiation is determined by COADS cloudiness, surface air temperature (SAT) and air humidity, and model SST. The sensible heat is formulated according to the difference of COADS SAT and model SST. The latent heat is calculated from the difference of COADS air humidity and saturated humidity at model SST (Gill 1982). The sea surface salinity is restored to the monthly Levitus (1982) climatology with a restoring time of 100

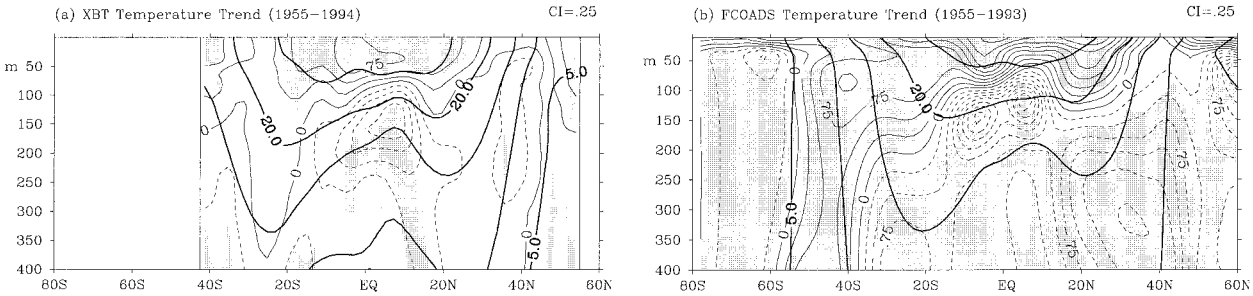

FIG. 2. Linear trend (1955–93) of zonal average (120°E–70°W) temperature in the Pacific Ocean for (a) WBW data and (b) FCOADS run. The CIs are 0.5 K century^{-1}. Shaded region indicates that the confidence level is higher than 95%. The heavy solid contours indicate the mean temperature distribution, and their CI is 5°C.

days. The initial temperature and salinity are set to the Levitus annual mean temperature and salinity. The model is spun up for 500 yr using monthly COADS data of 1945, and is then integrated for another 49 yr with monthly COADS data from 1945 to 1993 (FCOADS run hereinafter).

The monthly mean COADS data (1945–93) are produced by objective analysis of observations with a resolution of 1° × 1° (da Silva et al. 1994). The primary atmospheric variables such as SAT, air humidity, wind velocities, and total cloudiness are used to force the ocean. The linear trend and associated uncertainty of SST, net surface heat flux, and total cloudiness are analyzed (Figs. 1a–c). The COADS winds are corrected at a reduction rate of 50% century^{-1} according to Clarke and Lebedev (1996, 1997), Cardone et al. (1990), Ramage (1987), Posmentier et al. (1989), Ward (1992), and Ward and Hoskins (1996). The reason is that the historical wind observations had a systematic bias toward higher speed owing to the change of observational instruments from the Beaufort estimation at 10 m to a mean platform height of 20 m. This correction was not considered in the COADS. Corrected surface winds have a weakening trend in both the tropical Pacific and midlatitude North Pacific (Fig. 1d), consistent with Curtis and Hastenrath (1999).

3. Temperature trend

a. Latitudinal distribution

The zonal averaged (120°E–70°W) temperature trend in the upper Pacific Ocean is illustrated in Fig. 2a, using objectively analyzed data (White 1995; WBW data hereinafter). A warming trend near the surface but a cooling trend in the subsurface are shown at all latitudes. The tropical Pacific contains a warming trend of about 0.5 K century^{-1} above 100 m but a cooling trend of about 1.0 K century^{-1} below 100 m between 20°S and 20°N. The cooling is centered within the 15°–20°C isotherms or middle thermocline. A warming of about 0.5 K century^{-1} occurs north of 45°N in the upper 100 m and extends to 400 m. Near 40°N, the surface warming is weak, but the subsurface ocean is dominated by a cooling below 50 m. In the subtropical South Pacific between 40° and 20°S, a warming trend of about 0.5 K century^{-1} above 100 m and a weak cooling trend below 200 m are indicated.

An important issue regarding to the temperature trends is their statistical significance (see Walpole and Myers 1985). We notice that the confidence level of the zonal averaged temperature trend is not very high in most regions in the WBW data. However, it is important to note that the opposite trends in the western and eastern Pacific largely cancel each other (see sections 3b and 3c), causing the zonal average temperature trend to be weaker and statistically less confident.

The FCOADS simulation (Fig. 2b) is in fairly good agreement with the WBW data. The pattern of temperature trends in the WBW data is well simulated. The pattern correlation coefficient between the simulation and WBW data is 0.62. The magnitude of warming and cooling trends, however, is larger in the simulation than in the WBW data. The warming below 50 m north of 40°N in the WBW data is not shown in the simulation.

b. Tropical Pacific

The temperature trends also have significant zonal variation. The WBW data show that the tropical Pacific (averaged between 10°S and 10°N) is characterized by a warming trend near the surface. In the thermocline, the eastern Pacific exhibits a warming trend while the western Pacific shows a cooling trend, implying a flattening of the equatorial thermocline (Fig. 3a). The warming trend is about 1.5 K century^{-1} east of 150°W above 150 m, and the cooling trend is about 2.0 K century^{-1} west of 150°W between 50 and 400 m.

The temperature trends in the WBW data are simulated very successfully in the FCOADS run (Fig. 3b). The pattern of the simulated temperature trends is consistent with the WBW data. Their pattern correlation coefficient is 0.81, although the magnitude of both the warming and cooling trends is larger in the simulation than in the WBW data.

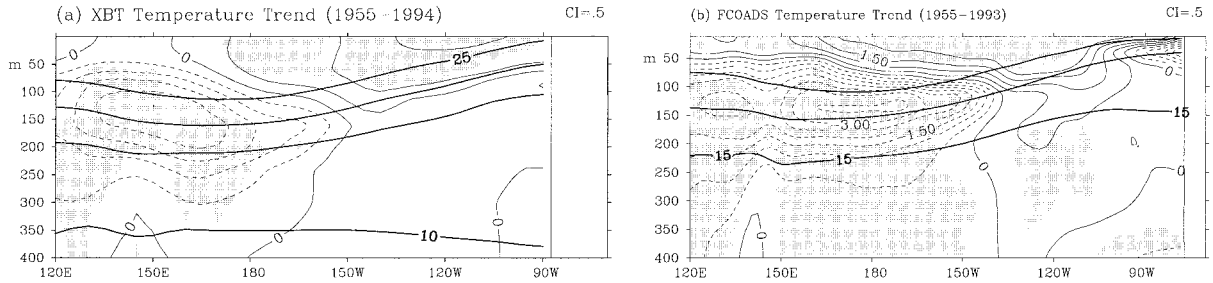

FIG. 3. Same as Fig. 2 but for the linear trend of average temperature in the tropical Pacific (10°S–10°N).

c. *Midlatitude North Pacific*

Consistent with the COADS SST observations (Fig. 1a), the WBW data suggest a warming trend of 2.0 K century^{-1} east of 150°W but a cooling trend of 0.5 K century^{-1} west of 150°W (Fig. 4a) in the upper 200 m of the midlatitude North Pacific (30°–50°N). The temperature trend beneath the 10°C mean isotherm is near zero.

The pattern of temperature trends in the WBW data is well simulated in the FCOADS run (Fig. 4b), with a pattern correlation coefficient of 0.61. However, the temperature trends are larger and located deeper in the simulation than in the WBW data. The warming and cooling trends in the deeper ocean are probably associated with the weaker thermocline in the simulation. The simulated temperature trends occur above the 10°C mean isotherm, as in the WBW data. However, the mean isotherm of 10°C is deeper in the simulation than in the WBW data, which implies excessive convection in the model. Excess diffusion in OGCMs is also well known to deepen isotherms.

To better understand the mechanisms controlling the oceanic temperature trend, another simulation is performed with the ''linear'' wind stress and surface heat fluxes. These linear fluxes are calculated from the linear trend of COADS atmospheric variables (LCOADS run hereinafter), in which the interannual variability is filtered out. The major features of the temperature trends in the WBW data are also simulated in the LCOADS run as shown in Huang (2000). However, the LCOADS run does not produce a temperature trend as clearly as in the FCOADS run, especially in the subsurface tropical ocean below 200 m. The pattern correlation coefficients are reduced to 0.47, 0.75, and 0.71, respectively, in the zonal (120°E–70°W), tropical (10°S–10°N), and subtropical (30°–50°N) average. The poorer simulation suggests that the interannual and decadal variability of surface forcing may contribute to the temperature trend.

In short, the WBW data indicate that the tropical Pacific exhibits a warming trend near the surface and in the thermocline of the eastern Pacific, but a cooling trend in the thermocline of the western Pacific. The midlatitude North Pacific is warmed in the east, but cooled in the west. These features are simulated reasonably in both the FCOADS and LCOADS simulations. The reasonable model simulation also gives us confidence that the heat budget in the model simulation is relevant to the temperature trends in the WBW data. This heat budget analysis should shed light on the causes of the temperature trends.

4. Heat budget in tropical Pacific

a. *Surface heat flux budget*

We start with the surface tropical Pacific (10°S–10°N) where a preliminary analysis has been carried out by Liu and Huang (2000). The mean (1945–93) net surface heat flux into the ocean is calculated as

$$Q_{\text{Net}} = S_0 + H_L + H_S + H_{\text{IR}}. \quad (1)$$

Here, S_0 represents downward solar radiation, and H_L, H_S, and H_{IR} represent latent, sensible, and infrared radiation heat fluxes, respectively. In the FCOADS run (Fig. 5a), the simulated mean incoming solar radiation

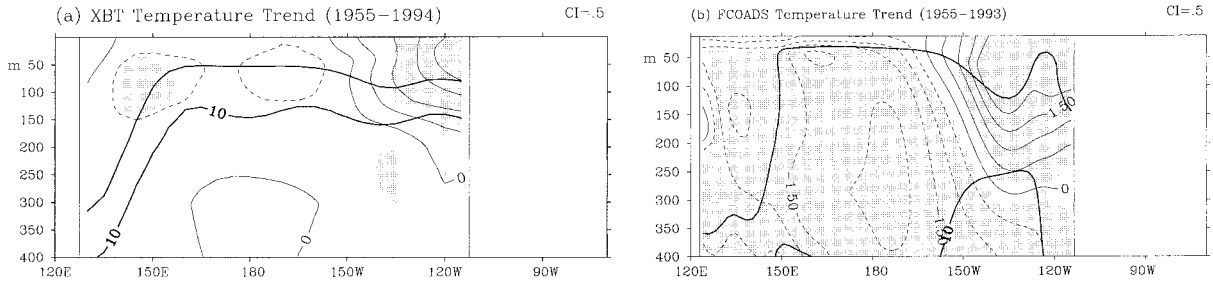

FIG. 4. Same as Fig. 2 but for the linear trend of average temperature in the midlatitude North Pacific (30°–50°N). The CI of mean thermocline is 2°C.

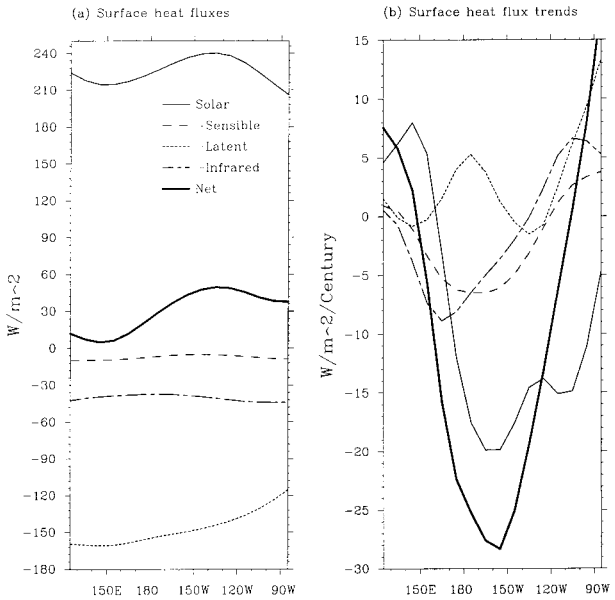

FIG. 5. (a) Mean surface heat fluxes (W m^{-2}, 1945–93) in the FCOADS run in the tropical Pacific (averaged in 10°S–10°N). (b) Trends of surface heat fluxes (W m^{-2} century^{-1}).

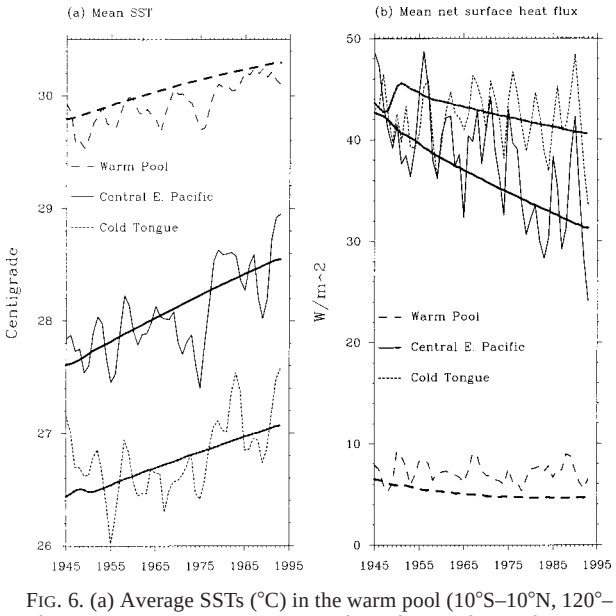

FIG. 6. (a) Average SSTs (°C) in the warm pool (10°S–10°N, 120°–170°E), central equatorial Pacific (10°S–10°N, 170°E–130°W), and cold tongue (10°S–10°N, 130°–70°W). (b) The average net surface heat flux (W m^{-2}) in the same regions. The thin and heavy lines represent the FCOADS and LCOADS runs, respectively. A 3-yr running mean is applied.

is balanced mainly by the cooling due to latent heat flux. The mean incoming solar radiation is the highest in the central Pacific, owing to low cloudiness in the COADS observations. The mean latent heat flux has the largest magnitude in the western Pacific, owing to the large air–sea humidity difference that is defined as $q_{\text{air}} - q_s(\text{SST})$. The mean sensible and outgoing infrared radiation heat fluxes have no significant zonal variation. As a result, the mean net heat flux into the ocean surface is about 5 W m^{-2} west of 170°E, and about 40 W m^{-2} east of 160°W. The distribution of these mean heat fluxes is consistent with the previous study of Gent (1991).

In spite of the dominant role of solar radiation and latent heat in the mean heat flux balance, all four components appear to have a comparable contribution to the trend of net surface heat flux in the simulation (Fig. 5b). The incoming solar radiation strengthens west of 160°E owing to the reduction of cloudiness, but weakens east of 160°E owing to the enhancement of cloudiness (Fig. 1c). The cooling due to latent heat flux weakens in the central equatorial Pacific between 160°E and 150°W owing to decreased speed of the zonal trade wind (Fig. 1d). It also weakens in the eastern Pacific east of 120°W owing to decreased speed of the northwestward wind. Surprisingly, the cooling due to sensible heat flux increases in the central equatorial Pacific between 150°E and 120°W. The reason is that the air–sea temperature difference has a positive trend in this region (not shown). But, the cooling due to sensible heat flux decreases east of 120°W, because the air–sea temperature difference has a negative trend (not shown) and the speed of northwestward wind decreases (Fig. 1d). The cooling due to outgoing infrared radiation increases between 130°E and 140°W. The reason is that the cloudiness reduces between 130° and 170°E and the SST increases between 170°E and 140°W. The cooling due to outgoing infrared radiation weakens east of 140°W, because the effect of SST increase is overwhelmed by the enhanced cloudiness (Fig. 1c).

As shown in Figs. 5b and 1e, the simulated net heat flux into the ocean weakens in the tropical Pacific between 150°E and 110°W. Therefore, the negative trend of net surface heat flux should tend to reduce the SST in the tropical Pacific. The damping effect of net surface heat flux on the SST seems to be the result of different heat flux components in different regions. In the warm pool (10°S–10°N, 120°–170°E), the damping effect results mainly from increased cooling due to outgoing

TABLE 1. Linear trends (1945–93, W m^{-2} century^{-1}) of average heat flux components in the FCOADS run. The regions are defined in the text. The percentages are confidence levels, whose value larger than or equal to 99% is indicated with an asterisk.

	Net	Solar	Sensible	Latent	Infrared
Warm pool	−0.40 15%	5.5 87%	−1.5 98%	−0.29 8%	−4.0 *
Central E. Pacific	−23.6 *	−16.8 *	−5.7 *	3.6 44%	−4.5 *
Cold tongue	−0.19 3%	−13.1 *	2.1 91%	5.5 76%	5.3 *
Western midlat.	23.5 *	−7.7 *	5.0 *	22.8 *	3.4 *
Eastern midlat.	−4.7 92%	−7.1 *	−1.5 96%	4.5 88%	−0.55 33%

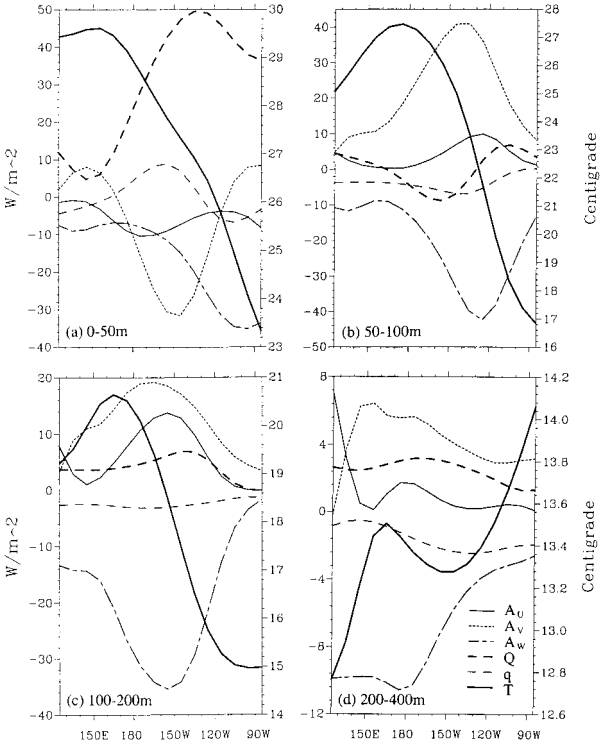

FIG. 7. Time (1945–93) and space (10°S–10°N, and depth) average temperature (°C, right coordinate) and terms of temperature equation (W m^{-2}, left coordinate) in the FCOADS run: (a) 0–50, (b) 50–100, (c) 100–200, and (d) 200–400 m.

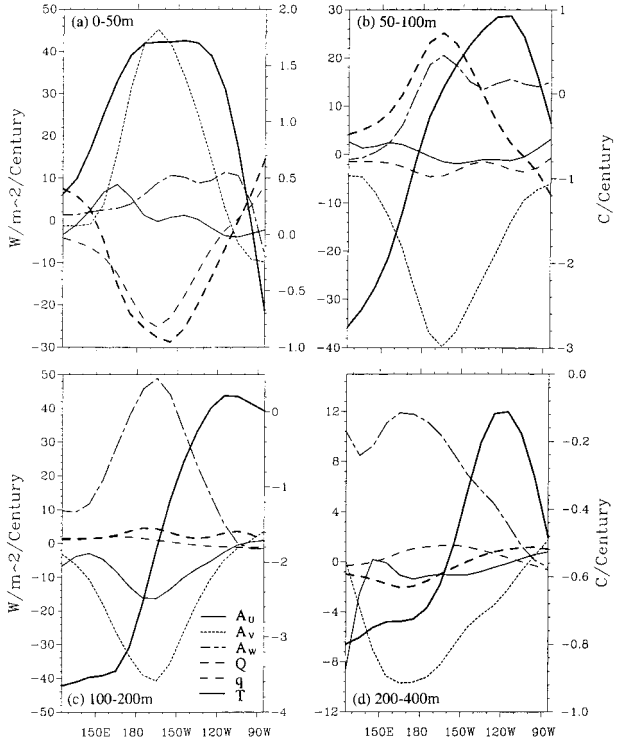

FIG. 8. Same as Fig. 7 but for the trends.

infrared radiation (Table 1) associated with the increase of SST and reduction of cloudiness. The damping effect also results from increased cooling due to sensible and latent heat fluxes associated with the increase of SST. As a result, the net heat flux decreases slightly, although the incoming solar radiation increases owing to the reduction of cloudiness. In the central equatorial Pacific (10°S–10°N, 170°E–130°W) and cold tongue (10°S–10°N, 130°–70°W), the damping effect results mainly from the reduction of incoming solar radiation associated with the enhancement of cloudiness (Table 1). The damping effect is further enhanced by increased cooling due to sensible and infrared radiation associated with a large increase of SST in the central equatorial Pacific. In the cold tongue, the damping effect becomes weaker since the cooling due to latent, infrared, and sensible heat fluxes becomes weaker. These fluxes in turn are associated with decreasing trade winds, increasing cloudiness, and reducing air–sea temperature difference.

The surface heat flux trends in the LCOADS run (not shown in detail) are very similar to those in the FCOADS run as discussed above. The negative feedback between net surface heat flux and SST is clearly indicated in both the FCOADS and LCOADS runs in the warm pool, central equatorial Pacific, and cold tongue regions (Figs. 6a,b). The average SST increases, while the net surface heat flux into the ocean decreases in all three regions in both runs. Therefore, the SST trend does not seem to be forced directly by the net surface heat flux.

b. Oceanic heat budget

To further investigate the mechanisms responsible for temperature trend in the surface and subsurface ocean, the simulated heat budget is diagnosed for the temperature equation in the surface (0–50 m) and subsurface (50–100, 100–200, and 200–400 m) layers ($i = 1, 4$):

$$\rho c_p H\left(\frac{\partial T}{\partial t}\right)_i = \rho c_p H(A_U + A_V + A_W)_i + Q_i + q_i. \quad (2)$$

Here

$$(A_U, A_V, A_W)_i = \left(-u\frac{\partial T}{\partial x}, -v\frac{\partial T}{\partial y}, -w\frac{\partial T}{\partial z}\right)_i \quad (3)$$

are vertical averaged advective heat fluxes, where Q_i and q_i are downward and upward turbulent heat fluxes, respectively, at the upper and lower ocean interfaces. For the 0–50-m layer, the upper interface is the ocean–atmosphere boundary, and therefore Q_1 is the net surface heat flux Q_{Net} in (1). The q_i flux is defined as

$$q_i = -Q_i + \rho c_p H\left(\gamma\frac{\partial^2 T}{\partial z^2} + \text{turbulence}\right)_i, \quad (4)$$

where *turbulence* represents the turbulent heat flux, γ

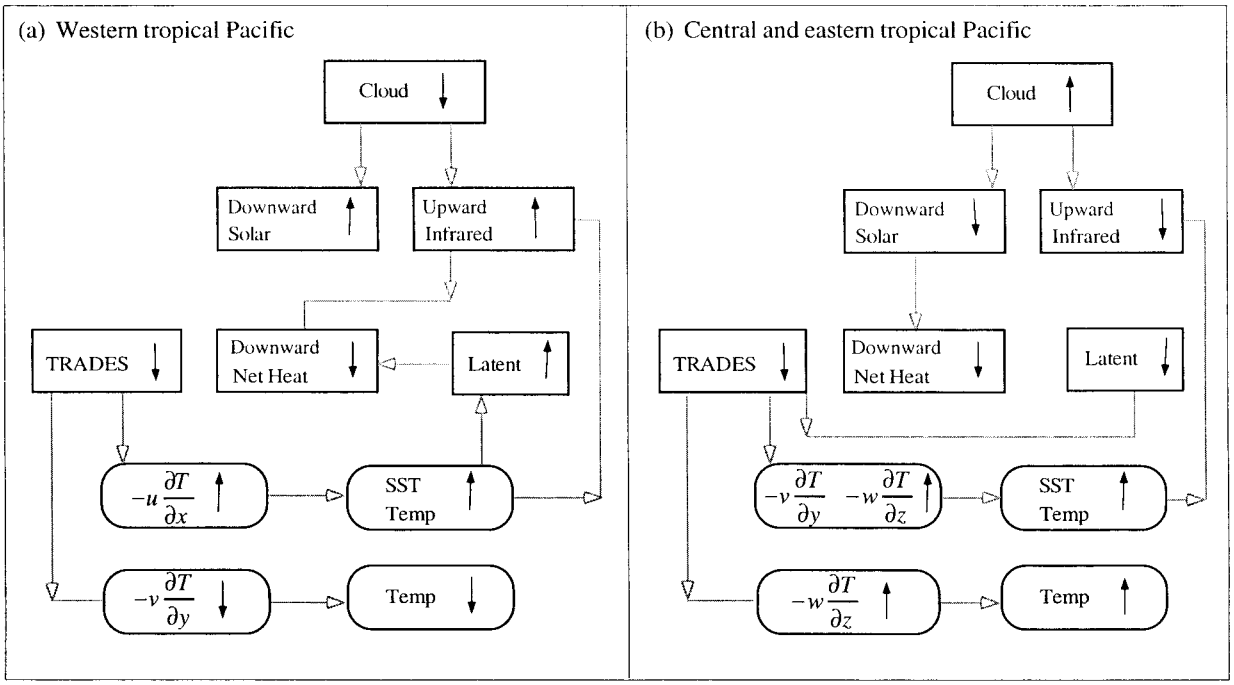

FIG. 9. Schematic mechanisms in (a) the western (120°–170°E) tropical Pacific and (b) the central and eastern (170°E–70°W) tropical Pacific. Upward (downward) arrows indicate increasing (decreasing). Round boxes indicate ocean variations, and shaded arrows indicate their association.

is the diffusivity, and $Q_i = q_{i-1}$ for the subsurface layers. Other notations are conventional.

The distribution of mean heat fluxes is reasonable in the FCOADS run. The cooling due to upwelling is the strongest near the eastern boundary in the surface layer (Fig. 7a). The strongest cooling is gradually shifted westward in the deeper layers (Figs. 7b–d), which might be associated with the westward deepening of the mean thermocline. The meridional advection is negative in the surface layer between 170°E and 110°W, owing to the divergent Ekman flow of the colder ocean temperature on the equator. The meridional advection becomes positive in the subsurface layers owing to the convergent geostrophic flow that compensates for the surface divergent Ekman flow (Wyrtki and Kilonsky 1984; Liu 1994). The longitude of maximum equatorward warm advection is also shifted toward the west at the deeper layers. The zonal advection is negative in the surface layer, which is associated with the transportation of cold water from the cold tongue by the South Equatorial Current (SEC). This westward cold advection is the strongest near 180°E owing to both a strong SEC and a modest zonal SST gradient on the edge of the warm pool. The zonal advection becomes positive in the deep layers owing to the eastward transport of the warm pool water by the Equatorial Undercurrent. The net turbulent heat flux becomes relatively smaller in the deeper layers (Figs. 7b–d), because turbulence occurs predominantly near the surface. In the equatorial thermocline (Figs. 7b–d), the mean cooling due to upwelling is balanced by the warming due to meridional and zonal advections. This suggests the dominant balance of adiabatic advection in the equatorial thermocline.

The trends of heat fluxes are diagnosed to help understand the temperature trends in the tropical Pacific at different longitudes and depths. The surface (0–50 m) tropical Pacific warms at a rate of about 1.5 K century^{-1} between 180° and 130°W (Fig. 8a). The warming may mainly result from reduced off-equatorial cold advection in the central equatorial Pacific (180°–120°W), reduced cooling due to upwelling in the eastern Pacific (east of 120°W), and reduced westward cold advection in the western Pacific (west of 180°E). Heat fluxes from the atmosphere and from below 50 m have a negative trend over the equatorial Pacific, which implies that the increasing ocean temperature is associated more directly with the ocean advective heat fluxes.

The reduction of cold advection in the tropical Pacific Ocean seems to be associated with the reduced trade winds (Fig. 1d). The weakening of the westward trade wind reduces the surface SEC, the off-equatorial divergent Ekman flow, and the upwelling in the central and eastern Pacific. Therefore, we conclude that the increasing temperature of the surface tropical Pacific is not associated directly with the net surface heat flux, but results from the reduction of the westward trade winds.

In the layer of 50–100 m, the effect of reduced cooling due to upwelling contributes predominantly to the warming trend in the eastern Pacific (Fig. 8b). In con-

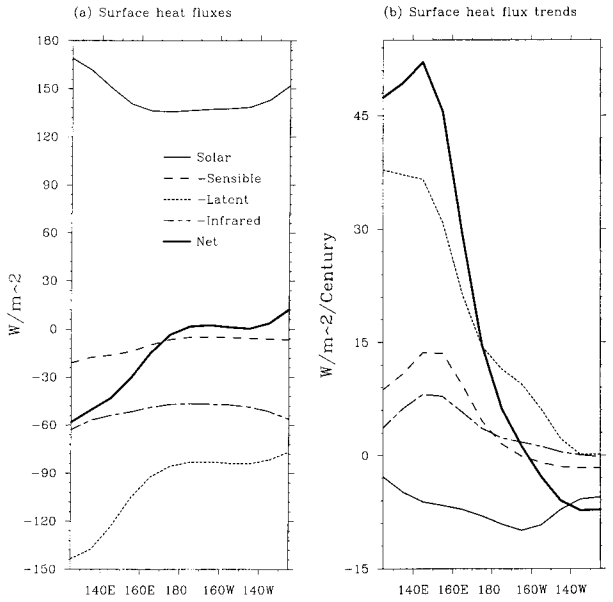

FIG. 10. (a) Means surface heat fluxes (W m^{-2}, 1945–93) in the FCOADS run in the subtropical North Pacific (30°–40°N). (b) Trends of surface heat fluxes (W m^{-2} $century^{-1}$).

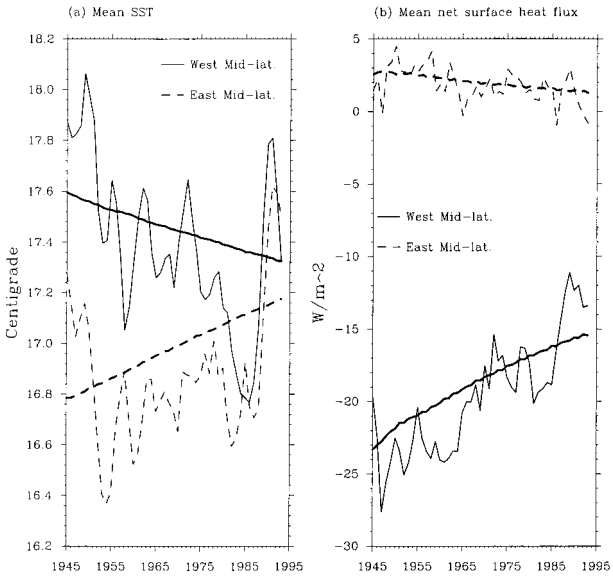

FIG. 11. (a) Average SSTs (°C) in the western (30°–40°N, 120°E–160°W) and eastern (30°–40°N, 160°–110°W) North Pacific. (b) Average net surface heat flux (W m^{-2}) in the same regions. The thin and heavy lines represent the FCOADS and LCOADS runs, respectively. A 3-yr running mean is applied.

trast, the cooling trend west of 180°E and below 50 m (Figs. 8b–d) is associated dominantly with reduced equatorward warm convergent flow. The upwelling and convergent flow are reduced owing to the weakening trade winds.

In short, the analysis of simulated heat budget suggests that the temperature trend in the tropical Pacific is associated directly with the oceanic advective heat fluxes, which in turn are forced by the trade winds. The reduction of the SEC and off-equatorial divergent flow causes the surface warming in the warm pool and central Pacific. The reduction of the equatorward warm convergent flow leads to the cooling trend in the thermocline of the western Pacific. The reduction of the upwelling causes the warming trend in the eastern Pacific. The associations between these oceanic changes and the reduction of the atmospheric trade winds are shown schematically in Fig. 9.

5. Heat budget in the midlatitude North Pacific

The midlatitude North Pacific (30°–50°N) contains two dynamically distinct regions: the subpolar gyre north of about 40°N and the subtropical gyre to the south. The heat budget between 30° and 40°N will be diagnosed first.

a. Surface heat flux budget

In the FCOADS run, the mean (1945–93) net surface heat flux is negative west of 180°E but slightly positive east of 180°W (Fig. 10a). The zonal distribution of the net surface heat flux is mainly determined by strong latent heat flux west of 160°E owing to the large air–sea humidity difference (not shown). The incoming solar radiation, sensible, and infrared radiation fluxes are relatively uniform in zonal distribution.

Opposite to the SST trend, the net surface heat flux exhibits a strong positive trend (50 W m^{-2} $century^{-1}$) west of 180°E but a weak negative trend (10 W m^{-2} $century^{-1}$) east of 180°W (Fig. 10b). The positive trend in the west seems to be associated mainly with the reduced cooling due to latent heat flux, which in turn is associated with the decrease of westerly wind speed and the air–sea humidity difference. The negative trend in the east is mainly caused by the reduction of incoming solar radiation, which is related to the enhanced cloudiness (Fig. 1c). The fact that the trend of net surface heat flux is opposite to the SST trend suggests that the surface heat flux has a damping effect on the SST trend. This is the same as in the tropical Pacific in section 4a.

A more detailed heat budget is shown in Table 1 for the FCOADS simulation. It suggests that the damping effect of the net surface heat flux on the SST trend results from different factors at different regions. The damping effect is caused by reduced cooling due to latent heat flux in the western Pacific (150°E–160°W) but by reduced warming due to solar radiation in the eastern Pacific (160°–110°W). The net surface heat flux increases in the western Pacific, because the reduction of latent heat, sensible heat, and outgoing infrared radiation heat fluxes exceeds that of the solar radiation. The reduction of the latent and sensible heat results from the reduction of the westerly wind speed (Fig. 1d), the air–sea humidity difference, and the air–sea temperature

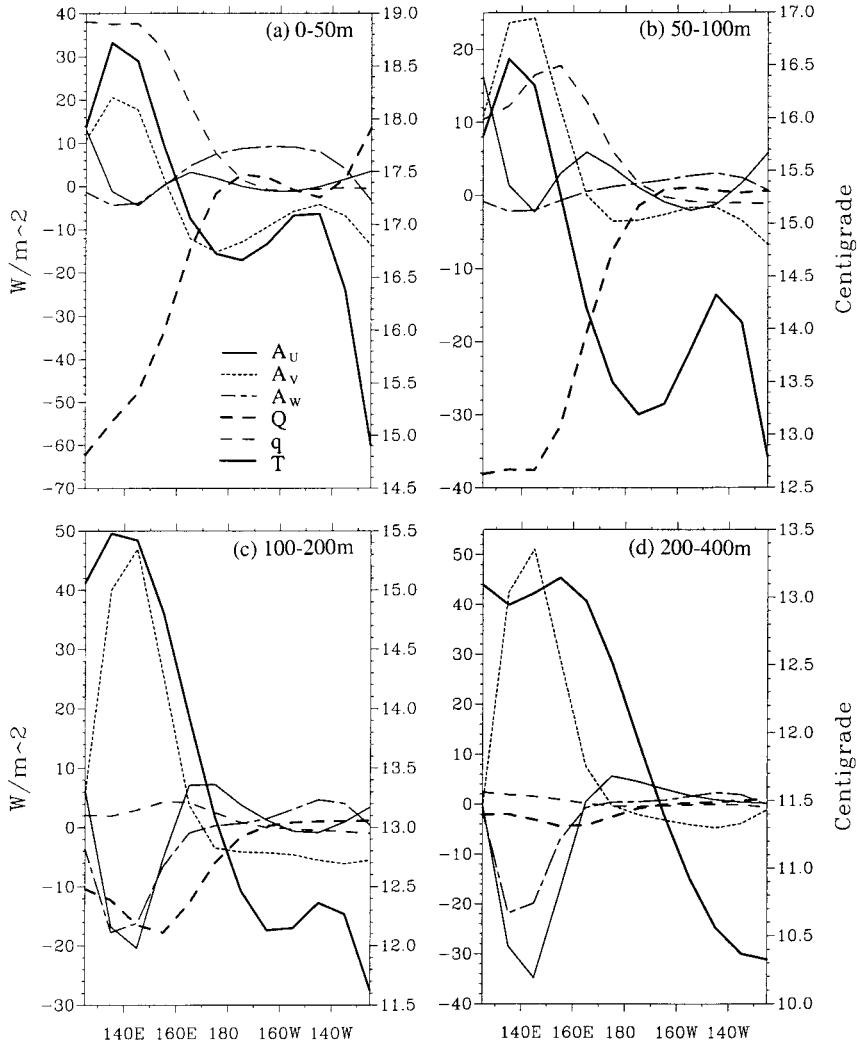

FIG. 12. Time (1945–93) and space (30°–40°N, depth) average temperature (°C, right coordinate) and terms of temperature equation (W m^{-2}, left coordinate) in the FCOADS run: (a) 0–50, (b) 50–100, (c) 100–200, and (d) 200–400 m.

difference (not shown). The reduced cooling due to outgoing infrared radiation is associated with increasing cloudiness and decreasing SST. In the eastern Pacific, the incoming solar radiation is reduced owing to the increase of cloudiness. Likewise, the latent and outgoing infrared heat fluxes are also reduced. The reduction of latent heat flux is associated with the reduction of the surface wind speed, since the air–sea humidity difference increases slightly. The reduction of outgoing infrared radiation is related to the enhancement of cloudiness. The total reduction of latent and outgoing infrared heat flux is not large enough to compensate the reduction of solar radiation, and therefore the downward net heat flux decreases.

The surface heat budget of the midlatitude North Pacific is very similar in the LCOADS run (not shown in detail). The opposite trends of SST and surface heat fluxes can be seen clearly from the SST and net surface heat flux averaged in the western Pacific and eastern Pacific in both the FCOADS and LCOADS runs (Figs. 11a,b). The SST decreases but the net surface heat flux increases in the western Pacific. In contrast, the SST increases but the net surface heat flux decreases in the eastern Pacific.

b. Oceanic heat budget

The zonal distributions of mean temperature and its terms in (1) are well understood in the FCOADS run (Figs. 12a–d). The mean ocean temperature is higher in the west than in the east, which is associated with the subtropical gyre circulation and the Kuroshio. The mean meridional advection is northward within the Kuroshio (west of 160°E) but southward east of 160°E. The reasons for the southward advection are that the Ekman transport is southward in the surface layer and the Sver-

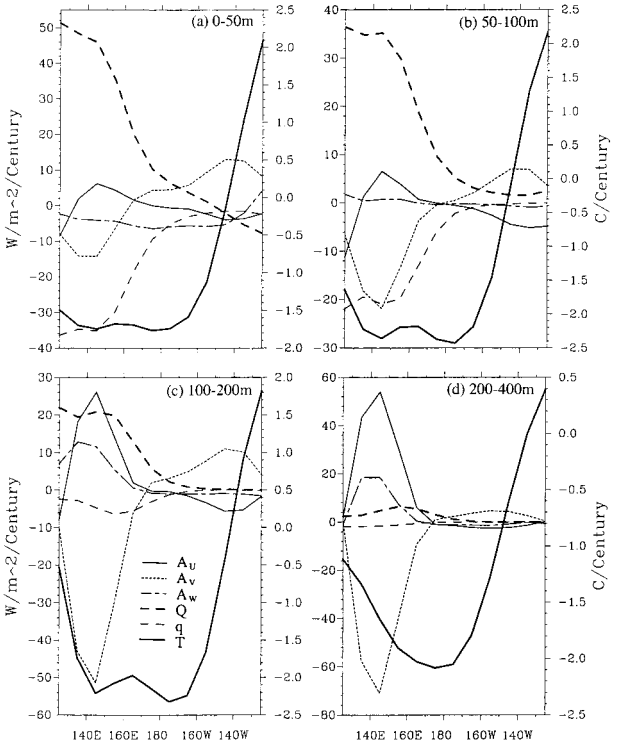

FIG. 13. Same as Fig. 12 but for the trends.

drup flow is southward in the subsurface layers in the subtropical gyre. The mean turbulent heat flux is very strong west of 180°E and penetrates downward to about 200 m. The upward and eastward cold advection between 130° and 160°E below 100 m might directly be associated with the Kuroshio in the western boundary.

As in the tropical ocean, the temperature change in the midlatitude North Pacific looks to be associated with ocean advection. The FCOADS simulation shows that the subtropical ocean warms east of 150°W between 0 and 200 m but cools west of 150°W (Figs. 13a–d). The warming east of 150°W is mainly related to the reduced southward cold advection. The reasons are the decrease of westerlies for the surface layer (0–50 m) and the decrease of wind stress curl (see Fig. 1d) for the water beneath the Ekman layer (below 50 m). The cooling west of 160°E is associated with the reduction of northward warm advection of the Kuroshio (0–400 m), which in turn may result from the reduced wind stress curl in the subtropical gyre.

Between 40° and 50°N (not shown), the mean temperature is colder in the west than in the east owing to the cyclonic gyre circulation and the Oyashio. The meridional advection is southward in the surface layer owing to the southward Ekman flow. However, it is northward in the subsurface layers west of 160°W owing to the Sverdrup flow, but it is kept southward in the subsurface layers east of 160°W owing to the northward penetration of the subtropical gyre. The mean vertical velocity west of 160°W is upward owing to the positive wind stress curl. This leads to the upward warm advection during the winter season when the surface temperature is slightly colder than the subsurface temperature.

Further, in the surface layer (0–50 m) between 40° and 50°N, the increase of ocean temperature east of 150°W is associated with the reduction of southward cold advection owing to the reduced westerlies. The decrease of ocean temperature west of 150°W may result from the reduction of upward warm advection. In the subsurface layer below 50 m, the increase of ocean temperature east of 150°W is related to the reduced southward cold advection. The reason is that the wind stress curl reduces within the subtropical gyre. The decrease of temperature west of 150°W appears to be associated with the reduction of northward warm advection owing to the reduction of northward Sverdrup flow within the subpolar gyre.

In short, the OGCM simulation suggests that the cooling in the western Pacific of the midlatitude and the warming in the eastern North Pacific of the midlatitude are associated with the oceanic advective heat fluxes. These advective heat fluxes in turn are controlled dynamically by the reduction of the westerlies. The mechanisms discussed above are summarized schematically in Fig. 14.

6. Discussion

a. Dynamic effect on tropical SST

We have demonstrated why the tropical SST increases despite a decreasing downward net surface heat flux. The major factor controlling the SST trend might be the oceanic advective heat fluxes, which in turn are controlled by the trade winds. The mechanisms between the SST and trade winds are consistent with the coupled model study of Liu and Huang (1997).

Hartmann and Michelsen (1993) pointed out that the large-scale atmospheric circulation can exert a dynamic regulation of tropical SST by adjusting the boundary-layer humidity through convergence and divergence. Wallace (1992) and Pierrehumbert (1995) also emphasized that the atmospheric circulation has a major effect on the regulation of tropical SST. These studies have focused on the ocean–atmosphere interface. Less attention is paid to the subsurface and thermocline waters.

The effect of ocean dynamics on the regulation of SST has also been discussed in other studies (Clement et al. 1996; Seager and Murtugudde 1997). Their results show that the increase of SST is reduced if ocean advection is considered, when the ocean is forced with a uniform global warming. In these studies, however, either the atmospheric winds are specified in a simple atmospheric mixed-layer model or the deeper ocean temperature is specified in an intermediate ocean–atmosphere model. In contrast, our study shows that the change of atmospheric winds has critical effect on the

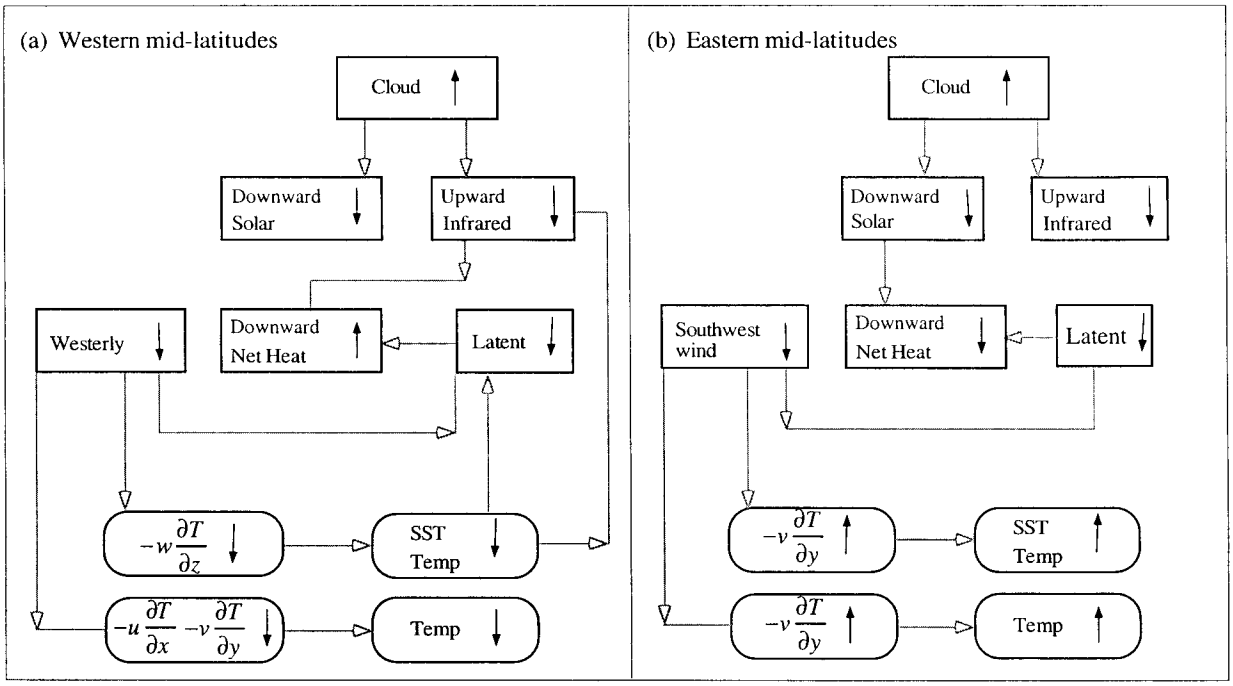

FIG. 14. Schematic mechanisms in (a) the western (120°E–160°W) and (b) the eastern (160°–110°W) subtropical (30°–40°N) North Pacific. Upward (downward) arrows indicate increasing (decreasing). Round boxes indicate ocean variations, and shaded arrows indicate their association.

ocean temperature trend. Our additional experiments show that the distribution of simulated ocean temperature trend remains similar to the FCOADS simulation, when the thermodynamic effects from cloudiness, SAT, and air humidity trends are shut off.

b. Thermodynamic effect on tropical SST

The important effect of ocean dynamics on the ocean temperature trend indicates that the negligence of oceanic advection is not as trivial as suggested by Ramanathan and Collins (1991). They hypothesized that the cirrus cloud can act as a thermostat regulating the maximum warm pool SST. This hypothesis does not seem to be valid in the long-term trends of the warm pool SST and cloudiness, because the SST increases while the cloudiness decreases over the warm pool. The enhancement of observed warm pool SST is not associated with the enhancement of cloudiness. As indicated in Fu et al. (1992) and Schneider et al. (1996), the cloudiness over the warm pool has little effect on the SST in the annual timescale, based on the observations and simulations of coupled ocean–atmosphere GCMs. Curtis and Hastenrath (1999) also concluded that there is no correlation between SST and cloudiness in the western Pacific warm pool during the boreal winter (their Fig. 4a). However, our study shows that the increase of SST is probably associated with increased cloudiness in the cold tongue region, which is consistent with the study of Curtis and Hastenrath (1999). In their study, however, it is not explained why the SST is increased in the cold tongue and warm pool regions. Our studies show that a reasonable explanation for the SST trend has to invoke oceanic processes.

Another thermodynamic regulator of the warm pool SST is the latent heat flux as proposed by Sarachik (1978) and Newell (1979). The increased incoming solar radiation owing to the reduction of cloudiness is completely compensated by the change of latent and infrared radiation heat fluxes in the warm pool during the past decades. Nevertheless, the enhancement of latent heat flux is not large enough to eliminate the warming trend in the warm pool. The enhancement of latent heat flux even becomes negligible in the cold tongue region, where the air–sea humidity difference does not increase very much.

7. Conclusions

Using the objectively analyzed data and OGCM simulations from 1955 to 1994, our conclusion is that the tropical Pacific Ocean has warmed near the surface west of 160°W and above 400 m east of 160°W but cooled in the thermocline west of 160°W between 50 and 400 m. The temperature gradient between the warm pool and cold tongue is reduced, which is consistent with the reduction of the trade winds owing to the weakening of the Walker circulation in the tropical Pacific. During this period, the midlatitude North Pacific between 30°

and 50°N is warmed east of 150°W above 200 m but cooled west of 160°W above 300 m.

One of the most interesting results is that the trends of SST are largely opposite to those of net surface heat flux in both the tropical Pacific and the midlatitude North Pacific. Therefore, ocean advective heat fluxes are of critical importance to the SST trends. More specific, the temperature trends may be directly associated with the reduction of the trade winds and the resultant ocean advective heat fluxes in the tropical Pacific. The reduction of westward trade wind decreases the cold advection of the SEC and the off-equatorial divergent flow and results in the surface warming in the warm pool and central Pacific. In the mean time, the equatorward convergent flow decreases in the thermocline. Thus, the equatorward warm advection decreases, which results in the cooling in the western Pacific thermocline. In the eastern Pacific, the reduction of northwestward trade wind decreases the cooling due to upwelling and results in a warming.

In the western North Pacific of the midlatitude (west of 160°E, 30°–40°N), the cooling appears to be associated with the weakening of the northward warm Kuroshio. In the eastern North Pacific of the midlatitude (east of 150°W, 30°–50°N), the warming looks to be associated with the reduced southward cold advection. The reasons are that the southward Ekman flow reduces in the surface layer and the southward Sverdrup flow reduces in the subsurface ocean.

Our study is consistent with other studies. For example, the surface warming in the eastern tropical Pacific is consistent with recent stronger El Niño events. The damping effect of net surface heat flux on SST is also observed during the El Niño events (Wang and McPhaden 2000). However, our study is only an oceanic perspective about the ocean temperature trend. We are unable to answer why the trade winds are weakening, since the trade winds and SSTs are coupled to each other in nature. The reduction of the trade winds is associated with the change of global atmospheric circulation, which may largely be forced by the SSTs. It has to be noted that the weakening of the trade winds in our analysis of COADS is inconsistent with the conclusion of Latif et al. (1997). Their simulation of an atmospheric GCM forced with observed SSTs indicates that the trade winds strengthen in the past decades, which appears to be consistent with the *uncorrected* COADS winds. However, their simulation cannot explain why the trade winds strengthen while the tropical SST gradient decreases.

We should also point out that the linear temperature trends between 1945 and 1994 are robust in the WBW data, although the observations before the late 1960s are relatively sparse. More analysis indicates that the patterns of the temperature trends between 1968 and 1994 do not have qualitative change, except that the magnitude of warming and cooling becomes larger. The statistical confidence does not seem to be reduced, since the magnitude of the trends becomes larger although the number of data becomes less. The increase of the trend magnitude seems to be reasonable. As the timescale representing the trends becomes shorter, the local variability is increased. However, we should be cautious that the temperature trends presented in this paper might be a part of oscillation of longer time period. Indeed, the tropical SST seems to exhibit a cooling trend in the first half of the century as indicated by Curtis and Hastenrath (1999) and implied in Cane et al. (1997). The questions of interest are: Will the trade winds stop decreasing and the tropical SSTs cool down again in the future? Will the change of atmospheric circulation be associated with the CO_2-induced global warming? Further studies need to be done with the coupling of the atmosphere and ocean.

Acknowledgments. The authors are in debt to Dr. W. B. White of Scripps Institution of Oceanography, University of California, San Diego, who provided us the objectively analyzed dataset. We appreciate the helpful discussions with Drs. Stefan Hastenrath, John Kutzbach, and John Young of University of Wisconsin—Madison in the earlier version of our paper. The comments from Dr. M. E. Mann of University of Virginia and three anonymous reviewers contributed greatly to the revision of the paper.

REFERENCES

Cane, M. A., A. C. Clement, A. Kaplan, Y. Kushnir, D. Pozdnyakov, R. Seager, S. E. Zebiak, and R. Murtugudde, 1997: Twentieth-century sea surface temperature. *Science,* **275,** 957–960.

Cardone, V. J., J. G. Greenwood, and M. A. Cane, 1990: On trends in historical marine wind data. *J. Climate,* **3,** 113–127.

Chepurin, G. A., and J. A. Carton, 1999: Comparison of retrospective analyses of the global ocean heat content. *Dyn. Atmos. Oceans,* **29,** 119–145.

Clarke, A. J., and A. Lebedev, 1996: Long-term changes in the equatorial Pacific trade winds. *J. Climate,* **9,** 1020–1029.

——, and ——, 1997: Interannual and decadal changes in equatorial wind stress in the Atlantic, Indian, and Pacific Oceans and the eastern ocean coastal response. *J. Climate,* **10,** 1722–1729.

Clement, A. C., R. Seager, M. A. Cane, and S. Z. Zebiak, 1996: An ocean dynamical thermostat. *J. Climate,* **9,** 2190–2196.

Curtis, S., and S. Hastenrath, 1999: Long-term trends and forcing mechanisms of circulation and climate in the equatorial Pacific. *J. Climate,* **12,** 1134–1144.

da Silva, A. M., C. C. Young, and S. Levitus, 1994: *Atlas of Surface Marine Data 1994.* NOAA Atlas NESDIS 6–8, 912 pp.

Fu, R., A. D. Genio, W. B. Rossow, and W. T. Liu, 1992: Cirrus-cloud thermostat for tropical sea surface temperatures tested using satellite data. *Nature,* **358,** 394–397.

Gent, P. R., 1991: The heat budget of TOGA-CORE domain in ocean model. *J. Geophys. Res.,* **96,** 3323–3330.

Giese, B. S., and J. A. Carton, 1999: Interannual and decadal variability in the tropical and midlatitude Pacific Ocean. *J. Climate,* **12,** 3402–3418.

Gill, A. E., 1982: *Atmosphere–Ocean Dynamics.* Academic Press, 662 pp.

Hartmann, D. L., and M. L. Michelsen, 1993: Large-scale effects on the regulation of tropical sea surface temperature. *J. Climate,* **6,** 2049–2062.

Huang, B., 2000: Understanding the temperature trends of the world

upper oceans. Ph.D. dissertation, University of Wisconsin–Madison, 142 pp. [Available from the Memorial Library, 728 State St., Madison, WI 53706.]

Knutson, T. R., and S. Manabe, 1998: Model assessment of decadal variability and trends in the tropical Pacific Ocean. *J. Climate,* **11,** 2273–2296.

Latif, M., R. Kleeman, and C. Eckert, 1997: Greenhouse warming, decadal variability, or El Niño? An attempt to understand the anomalous 1990s. *J. Climate,* **10,** 2221–2239.

Levitus, S., 1982: *Climatological Atlas of the World Ocean.* NOAA Prof. Paper 13, 173 pp. and 17 microfiche.

——, and R. D. Gelfeld, 1992: National Oceanographic Data Center inventory of physical oceanographic profiles. Key to oceanographic records documentation No. 18, NODC, NESDIS, 242 pp.

——, and T. Boyer, 1994: *Temperature.* Vol. 4, *World Ocean Atlas 1994*, NOAA Atlas NESDIS, 117 pp.

Liu, Z., 1994: A simple model of the mass exchange between the subtropical and tropical ocean. *J. Phys. Oceanogr.,* **24,** 1153–1165.

——, and B. Huang, 1997: A coupled theory of tropical climatology: Warm pool, cold tongue, and Walker Circulation. *J. Climate,* **10,** 1662–1679.

——, and ——, 2000: Cause of tropical Pacific warming. *Geophys. Res. Lett.,* **27,** 1935–1938.

Newell, R. E., 1979: Climate and the ocean. *Amer. Sci.,* **67,** 405–416.

Pacanowski, R. C., 1996: MOM2 documentation. GFDL Ocean Tech. Rep. 3.2, 329 pp.

Pierrehumbert, R. T., 1995: Thermostat, radiator fins, and the local runaway greenhouse. *J. Atmos. Sci.,* **52,** 1784–1806.

Posmentier, E. S., M. A. Cane, and S. E. Zebiak, 1989: Tropical Pacific climate trends since 1960. *J. Climate,* **2,** 731–736.

Ramage, C. S., 1987: Secular change in reported surface wind speeds over the ocean. *J. Climate Appl. Meteor.,* **26,** 525–528.

Ramanathan, R., and W. Collins, 1991: Thermodynamics regulation of ocean warming by cirrus clouds deduced from observations of the 1987 El Niño. *Nature,* **351,** 27–32.

Robinson, M. K., R. Bauer, and E. Schroeder, 1979: *Atlas of the North Atlantic–Indian Ocean Monthly Temperatures and Salinities of the Surface Layer.* Naval Oceanographic Office, NSTL, 211 pp.

Sarachik, E. S., 1978: Tropical sea-surface temperature: An interactive one-dimensional atmosphere ocean model. *Dyn. Atmos. Oceans,* **2,** 455–469.

Schneider, N., T. Barnett, M. Latif, and T. Stockdale, 1996: Warm pool physics in a coupled GCM. *J. Climate,* **9,** 219–239.

Seager, R., and R. Murtugudde, 1997: Ocean dynamics, thermocline adjustment, and regulation of tropical SST. *J. Climate,* **10,** 521–534.

Wallace, J. M., 1992: Effect of deep convection on the regulation of tropical sea surface temperature. *Nature,* **357,** 230–231.

Walpole, R. E., and R. H. Myers, 1985: *Probability and Statistics for Engineers and Scientists.* 3d ed. Macmillan, 639 pp.

Wang, W., and M. J. McPhaden, 2000: The surface layer heat balance in the equatorial Pacific Ocean. Part II: Interannual variability. *J. Phys. Oceanogr.,* **30,** 2989–3008.

Ward, M. N., 1992: Provisionally corrected surface wind data, worldwide ocean–atmosphere surface fields, and Sahelian rainfall variability. *J. Climate,* **5,** 454–475.

——, and B. J. Hoskins, 1996: Near-surface wind over the global ocean 1949–1988. *J. Climate,* **9,** 1877–1895.

White, W. B., 1995: Design of a global observing system for gyrescale upper ocean temperature variability. *Progress in Oceanography,* Vol. 36, Pergamon, 169–217.

Wyrtki, K., and B. Kilonsky, 1984: Mean water and current structure during the Hawaii–Tahiti shuttle experiment. *J. Phys. Oceanogr.,* **14,** 242–254.